An essential thioredoxin is involved in the control of the cell cycle in the bacterium *Caulobacter crescentus*

Received for publication, November 23, 2017, and in revised form, January 23, 2018 Published, Papers in Press, January 24, 2018, DOI 10.1074/jbc.RA117.001042

Camille V. Goemans[‡§¶1], François Beaufay[§2], Khadija Wahni[¶‖], Inge Van Molle[¶‖**3], Joris Messens[¶‖**4], and Jean-François Collet[‡§¶5]**

*From [‡]WELBIO, Avenue Hippocrate 75, 1200 Brussels, Belgium, the [§]de Duve Institute, Université catholique de Louvain, Avenue Hippocrate 75, 1200 Brussels, Belgium, the [¶]Brussels Center for Redox Biology, 1200 Brussels, Belgium, the [‖]Center for Structural Biology, Vlaams Instituut voor Biotechnologie (VIB), 1050 Brussels, Belgium, and **Structural Biology Brussels, Vrije Universiteit Brussel, 1050 Brussels, Belgium*

Edited by Ursula Jakob

Thioredoxins (Trxs) are antioxidant proteins that are conserved among all species. These proteins have been extensively studied and perform reducing reactions on a broad range of substrates. Here, we identified *Caulobacter crescentus* Trx1 (CCNA_03653; *Cc*Trx1) as an oxidoreductase that is involved in the cell cycle progression of this model bacterium and is required to sustain life. Intriguingly, the abundance of *Cc*Trx1 varies throughout the *C. crescentus* cell cycle: although the expression of *Cc*Trx1 is induced in stalked cells, right before DNA replication initiation, *Cc*Trx1 is actively degraded by the ClpXP protease in predivisional cells. Importantly, we demonstrated that regulation of the abundance of *Cc*Trx1 is crucial for cell growth and survival as modulating *Cc*Trx1 levels leads to cell death. Finally, we also report a comprehensive biochemical and structural characterization of this unique and essential Trx. The requirement to precisely control the abundance of *Cc*Trx1 for cell survival underlines the importance of redox control for optimal cell cycle progression in *C. crescentus*.

Thioredoxins (Trxs)[6] are small antioxidant proteins that have been identified in most living organisms. They receive electrons from NADPH through the flavoprotein-thioredoxin reductase and catalyze the reduction of oxidized cysteine residues in substrate proteins (1). As such, they are implicated in a variety of processes, ranging from oxidative stress defense to signal transduction. These soluble proteins all share a similar structure, a Trx fold consisting of five β-strands surrounded by four α-helices. They also display a strictly conserved WCGPC catalytic active-site motif and contain a *cis*-proline residue (1). The two cysteines of the catalytic motif are the key players involved in the reduction of oxidized substrates.

First identified in 1964 as an electron donor for ribonucleotide reductase (2, 3), *Escherichia coli* Trx1 (*Ec*Trx1) is a major cytoplasmic reductase that provides electrons to more than 260 substrates (4). To date, many bacterial Trxs have been characterized, and most share the same function as *Ec*Trx1. Here, we investigated *Caulobacter crescentus* Trx1 (CCNA_03653; *Cc*Trx1), a Trx protein with potentially two intriguing features. First, whereas most previously identified bacterial Trxs are not essential because of the presence of redundant reducing pathways, the gene encoding *Cc*Trx1 was identified as being essential in a large-scale transposon analysis (5). Second, a high-throughput gene-expression profiling experiment suggested that the transcription of *cctrx1* was cell cycle–regulated (6). Thus, these two observations led us to postulate that *Cc*Trx1 could play a unique role in *C. crescentus*.

The non-pathogenic α-proteobacterium *C. crescentus* is a favorite model organism to study cell cycle and division because of its asymmetric cell cycle and the clear separation between its G_1, S, and G_2/M phases (Fig. 1). Each cell cycle gives rise to two morphologically and functionally different daughter cells: a swarmer cell (in G_1 phase) and a stalked cell (in S phase) (for a review, see Ref. 7). The swarmer cell is motile and unable to initiate DNA replication. It has to differentiate into a sessile stalked cell (G_1 to S transition) before it is able to enter into a new replicative cycle (7) (Fig. 1). Conversely, the stalked cell initiates a new cell cycle shortly after cell division. In *C. crescentus*, this complex program is controlled by a handful of "master regulators," which themselves regulate the expression of more than 200 genes (7).

This work was supported in part by grants from Fonds de la Recherche Fondamentale Stratégique (FRFS)-WELBIO, European Research Council (FP7/2007–2013) ERC Independent Researcher Starting Grant 282335-Sulfenic, and grants from the Fonds de la Recherche Scientifique (FRS-FNRS). The authors declare that they have no conflicts of interest with the contents of this article.
This article contains Table S1 and Figs. S1–S3.
The atomic coordinates and structure factors (code 6ESX) have been deposited in the Protein Data Bank (http://wwpdb.org/).

[1] Fonds pour la Formation à la Recherche dans l'Industrie et dans l'Agriculture (FRIA) research fellow. To whom correspondence may be addressed: de Duve Institute Université catholique de Louvain, 75 Ave. Hippocrate, 1200 Brussels, Belgium. Tel.: 32-2-7646535; Fax: 32-2-7647598; E-mail: camille.goemans@uclouvain.be.
[2] Present address: Dept. of Molecular, Cellular, and Developmental Biology, University of Michigan, Ann Arbor, MI 48109.
[3] Supported by an Omics@VIB Marie Curie COFUND fellowship.
[4] Group leader at VIB. Supported by Hercules Foundation Equipment Grant HERC16 and Strategic Research Programme SRP34 of the Vrije Universiteit Brussel.
[5] "Directeur de Recherche" of the FRS-FNRS. To whom correspondence may be addressed: de Duve Institute, Université catholique de Louvain, 75 Ave. Hippocrate, 1200 Brussels, Belgium. Tel.: 32-2-7647562; Fax: 32-2-7647598; E-mail: jfcollet@uclouvain.be.

[6] The abbreviations used are: Trx, thioredoxin; *Ec*, *E. coli*; *Cc*, *C. crescentus*; TrxR, thioredoxin reductase; Grx, glutaredoxin; AMS, 4-acetamido-4′-maleimidylstilbene-2,2′-disulfonic acid; RNR, ribonucleotide reductase; Bis-Tris, 2-[bis(2-hydroxyethyl)amino]-2-(hydroxymethyl)propane-1,3-diol.

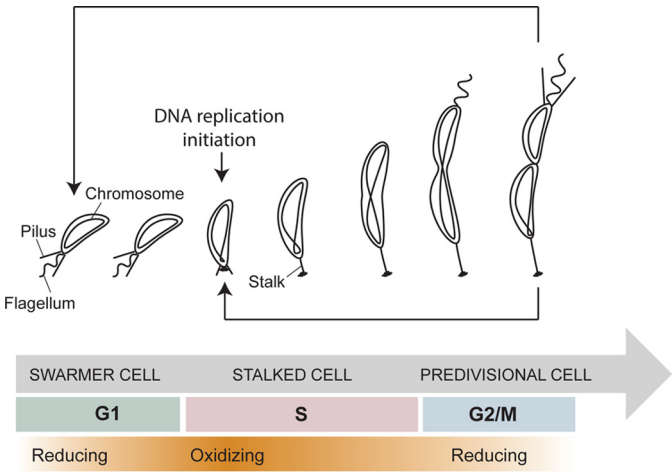

Figure 1. Schematic representation of the cell cycle of *C. crescentus*. The swarmer cell (in G_1 phase) differentiates into a stalked cell, which then initiates DNA replication (S phase). This leads to the formation of predivisional cells and division (G_2/M phase). The redox state of the cell fluctuates with more reducing (*white*) or oxidizing phases (*orange*) during the cycle.

Recently, using a redox-sensitive fluorescent probe, Narayanan *et al.* (8) demonstrated that the intracellular redox state of *C. crescentus* oscillated during the cell cycle. Indeed, the cytoplasm goes from reducing in the non-replicative G_1 cells to more oxidizing during the G_1 to S transition. Then, at mid-S phase, it gradually turns back to a more reduced state (Fig. 1). Moreover, the authors discovered that the regulatory protein NstA becomes activated by disulfide bond formation during the G_1 to S transition and showed that this activation directly depends on the redox state of the cells (8). These fluctuations are thought to act as a global switch that controls the cell cycle progression by fine-tuning the activity of regulatory proteins. Because the cell cycle is redox-regulated and Trxs are central players of the redox homeostasis network, we hypothesized that the activity of *Cc*Trx1 was connected to the cell cycle progression in this bacterium.

In this study, we demonstrated that *Cc*Trx1 displays the structural and biochemical properties of a classical reductase with a redox potential of −275 mV. Interestingly, we showed that *Cc*Trx1 is essential and that its abundance is tightly controlled, two features that are uncommon among bacterial Trxs. Expression levels of *Cc*Trx1 are not only controlled transcriptionally but also post-translationally; the protein is actively degraded by the ClpXP protease in predivisional cells. Thus, *Cc*Trx1 accumulates in early S phase when the cytoplasm of *C. crescentus* is more oxidizing and replication occurs. Modulating the levels of *Cc*Trx1 strongly interfered with cell growth and survival, thus confirming the physiological importance of this regulation. Altogether, our results shed light on the unusual activity of a classical Trx and uncover another layer of the complex redox regulation of the cell cycle in *C. crescentus*.

Results

CcTrx1 is a classical Trx

*Cc*Trx1 harbors the WCGPC catalytic motif and the conserved *cis*-proline found in all Trxs (Fig. 2*A*). To gain insight into the function of this protein, we investigated its redox properties. We first probed its oxidoreductase activity by testing its ability to catalyze the reduction of insulin by dithiothreitol (DTT) (9). Upon reduction, the A and B chains of insulin dissociate, and the B chain aggregates. This can be monitored by measuring the absorbance at 650 nm. The increase of the solution turbidity that is observed in the presence of *Cc*Trx1 confirms its oxidoreductase activity (Fig. 2*B*). We then measured the redox potential (E'_0) of *Cc*Trx1, a critical factor that determines the ability of a protein to either reduce or oxidize its substrates. By incubating *Cc*Trx1 in buffers containing different ratios of oxidized and reduced DTT, we calculated a redox potential of about −275 mV (Fig. 2*C*), a value that is similar to the redox potential of *Ec*Trx1 (−270 mV (10)). We next wondered whether *Cc*Trx1 could be recycled by the thioredoxin reductase expressed by *C. crescentus* (CCNA_02964; *Cc*TrxR). To address this question, we measured the K_m of *Cc*TrxR for *Cc*Trx1 using oxidized *Cc*Trx1 as a substrate in the presence of NADPH and obtained a K_m of 1.71 μM, indicating that *Cc*Trx1 is an excellent substrate for *Cc*TrxR (Fig. 2*D*). Thus, *Cc*Trx1 exhibits the classical features of a Trx *in vitro*.

CcTrx1 has a Trx fold with a more positively charged substrate contact surface compared with EcTrx1

To deepen our characterization of *Cc*Trx1, we solved its crystal structure and compared it with that of *Ec*Trx1. All crystallographic parameters are summarized in Table 1. *Cc*Trx1 shows a classical Trx fold, a single domain with a core formed of five β strands surrounded by four α-helices (Fig. 3*A*). Moreover, the structure of *Cc*Trx1 superimposes with the structure of *Ec*Trx1 (Protein Data Bank code 2TRX; 49% sequence identity) with a root mean square deviation of 0.617 Å for 96 atoms (Fig. 3*A*). The asymmetric unit contains three copies of *Cc*Trx1. In one chain, *Cc*Trx1 is present in the reduced form, whereas in the other two chains the electron density indicates the presence of a mixture of reduced thiols (75%) and a *CXXC* disulfide (25%).

As the structural fold of *Cc*Trx1 was identical to that of *Ec*Trx1 with an identical WCGPC rheostat active-site motif (11) (Fig. 3*B*), we decided to compare the electrostatic surface potential of *Cc*Trx1 with that of *Ec*Trx1. We found that *Cc*Trx1 has a more pronounced positive charge compared with the more neutral surface potential of *Ec*Trx1 (Fig. 3*C*). For comparison, we also used an *E. coli* protein with a glutaredoxin (Grx)-like structure but with Trx-like activity and that is responsible for the reduction of ribonucleotide reductase, *Ec*NrdH (12). *Ec*NrdH has an even more extreme positive contact surface area compared with *Cc*Trx1 (see "Discussion").

CcTrx1 is an essential protein

In vivo, Trxs are implicated in many different processes, mainly by maintaining their substrates in a reduced and active state under normal and oxidative stress conditions. Despite their critical function, most studied bacterial Trxs are not essential. This can be explained by the fact that most bacteria express redundant oxidoreductases with overlapping substrate specificity. In bacteria, there are two major reducing systems, the Trx and Grx pathways. In the Grx pathway, electrons flow from NADPH to glutathione via glutathione oxidoreductase. Reduced glutathione then provides electrons to Grx proteins,

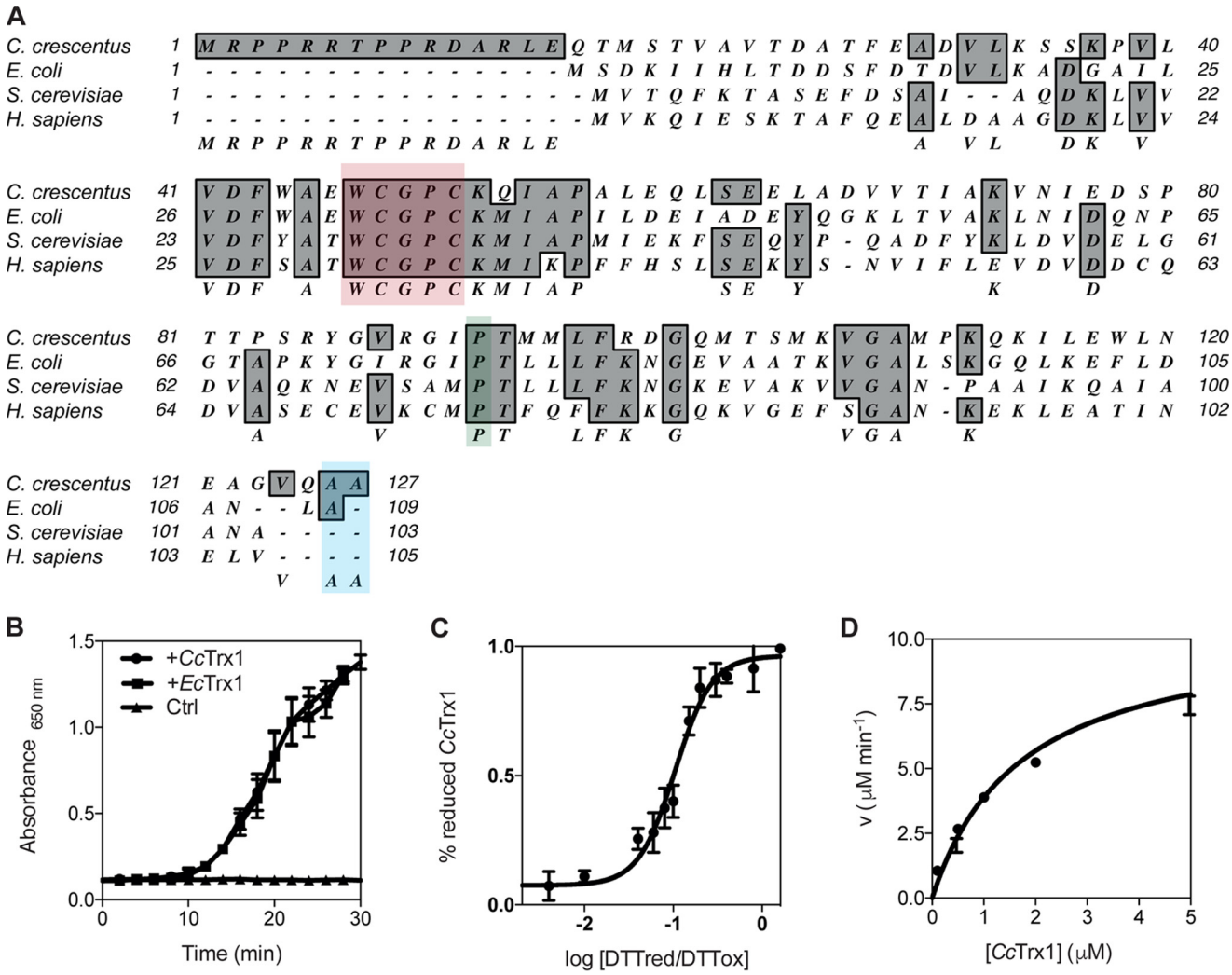

Figure 2. *Cc*Trx1 exhibits the biochemical properties of a classical Trx. *A*, alignment of *Cc*Trx1 with well studied Trxs from *E. coli* (NP_418228.2), *S. cerevisiae* (P22217), and *H. sapiens* (P10599.3) using MacVector 12.0.1. The catalytic WCGPC motif is highlighted in *red*, the *cis*-proline is in *green*, and the two C-terminal alanines are in *blue*. *B*, *Cc*Trx1 catalyzes the reduction of insulin by DTT as measured by following the increase in absorbance at 650 nm. *Ec*Trx1 was used as a positive control, and a sample without any Trx (*Ctrl*) was used as a negative control. This graph shows the mean of three independent experiments, and the *error bars* represent the S.E. *C*, the redox potential of *Cc*Trx1 is −275 mV. It was determined by equilibrating the protein in redox buffers containing different DTT_{red}/DTT_{ox} ratios. The redox potential was calculated from the ratio between the amounts of oxidized and reduced *Cc*Trx1 present at equilibrium and determined using AMS trapping experiments. The data shown are the mean ± S.E. of three independent experiments. *D*, the K_m of *Cc*TrxR for *Cc*Trx1 is 1.71 μM. The reduction of *Cc*Trx1 by *Cc*TrxR was monitored by measuring the decrease in absorbance at 340 nm, corresponding to the decrease in reduced NADPH (the experimental conditions are described under "Experimental procedures"). We measured the initial velocities (*v*) of *Cc*Trx1 reduction by *Cc*TrxR to determine the kinetic parameters of the reaction. This plot shows the mean ± S.E. of three independent experiments and a fit of the data to the Michaelis-Menten equation.

which in turn reduce their substrates (13). Although both pathways do not completely overlap, one can usually compensate for the absence of the other. Unexpectedly, *cctrx1* was annotated as being essential by a large-scale transposon study despite the presence of the Grx pathway in *C. crescentus* (5). To confirm this intriguing observation, we attempted to delete the *cctrx1* gene using a two-step recombination method classically used to produce deletion mutants in *C. crescentus*. In this method, a plasmid encoding the upstream and downstream homology regions of *cctrx1* as well as a kanamycin resistance cassette was transformed into WT cells (Fig. S1). Kanamycin selection led to the isolation of mutants that proceeded to the first recombination step and integrated the plasmid into their chromosome (Fig. S1). Because this plasmid also encodes a *sacB* gene, counterselection on sucrose led to the selection of mutants that proceeded to the second recombination step, thereby losing the plasmid (Fig. S1). For non-essential genes, the second recombination produces 50% deletion mutant clones and 50% WT clones (Fig. S1). In the case of *cctrx1*, all the clones recovered were WT, suggesting that this gene was indeed essential. Accordingly, we managed to delete the endogenous *cctrx1* (57% deletion clones) when an additional copy of *cctrx1* was ectopically integrated on the chromosome. Thus, we concluded that *Cc*Trx1 is essential, indicating that the role of this protein is so specific that it cannot be fulfilled by the other reducing proteins expressed by *C. crescentus*.

CcTrx1 is cell cycle–regulated

As mentioned before, numerous proteins cooperate in the tight control of the cell cycle of *C. crescentus*. To be active during their proper time window, these proteins usually exhibit a fluctuating expression profile during the cycle. Intriguingly, a

Table 1
X-ray data collection, processing, and refinement statistics

Data collection and processing	
Beamline	Proxima 2
Wavelength (Å)	0.980
Space group	P65
Unit cell	
a (Å)	85.1
b (Å)	85.1
c (Å)	105.0
$\alpha = \beta$ (°)	90
γ (°)	120
Resolution limits (Å)[a]	42.86–2.80 (2.97–2.80)
Total number of reflections	60,342 (9,632)
Number of unique reflections	10,793 (1,732)
Completeness (%)	99.7 (99.2)
Refinement statistics	
R_{meas} (%)	16.6 (112.4)
$\langle I/\sigma(I)\rangle$	11.55 (1.80)
R_{cryst}[b] (%)	18.76
R_{free}[c] (%)	27.02
Ramachandran profile	
Most favored (%)	99.39
Additionally allowed (%)	0.61
Disallowed (%)	0.00
r.m.s.[d] deviations	
Bond lengths (Å)	0.009
Bond angles (°)	1.216
Protein Data Bank code	6ESX

[a] Data in parentheses are for the highest-resolution shell.
[b] $R_{cryst} = \Sigma||F_{obs}| - |F_{calc}||/\Sigma|F_{obs}|$ where F_{obs} and F_{calc} are observed and calculated structure factor amplitudes, respectively.
[c] R_{free} as for R_{cryst} using a random subset of the data excluded from the refinement.
[d] Root mean square.

global transcription analysis (6) showed that the transcription of *cctrx1* was induced in the S phase. To verify whether this induction led to an increase in protein levels, we measured *Cc*Trx1 levels at different time points of the cell cycle after synchrony (14). Briefly, a mixed culture of *C. crescentus* was applied to a Ludox density gradient, which allows the separation of swarmer cells (higher density) from stalked and predivisional cells (lower density). These swarmer cells were collected and resuspended in fresh medium, allowing them to differentiate and divide simultaneously (14). Every 20 min, a sample was collected, and *Cc*Trx1 levels were assessed by immunoblotting (Fig. 4, *A* and *B*). MreB, which is expressed constitutively during the cell cycle, was used as a loading control, and CtrA, a protein involved in DNA replication inhibition and that is absent in stalked cells, served as a synchrony quality control (Fig. 4, *A* and *B*). Interestingly, this experiment clearly shows an increase in the abundance of *Cc*Trx1 in early S phase (Fig. 4, *A* and *B*).

CcTrx1 is a substrate of the ClpXP machinery

While assessing the levels of *Cc*Trx1 during the cell cycle (Fig. 4, *A* and *B*), we not only noticed an increase in *Cc*Trx1 levels in early S phase but also a severe decrease in predivisional cells. As Trxs are known to be extremely stable, we wondered what could cause such a decrease. We hypothesized that *Cc*Trx1 could be regulated at the post-translational level through cell cycle–dependent proteolysis. The careful analysis of the *Cc*Trx1 sequence (Fig. 2*A*) highlighted two alanines present at its C terminus, a motif often recognized by the ClpXP protease (15). The ClpXP machinery is an essential protein complex consisting of two different proteins, ClpX, an AAA+ ATPase, and ClpP, a peptidase. ClpX is responsible for the recognition, unfolding, and translocation of its substrates to ClpP (16). The ClpXP protease is responsible for the cell cycle–dependent degradation (17, 18) of key proteins (19–25), thereby confining their activities to specific phases of the cell cycle (26). To test whether the C-terminal AA motif triggers the degradation of *Cc*Trx1 by ClpXP, we assessed the cell-cycle expression profile of a *Cc*Trx1 mutant exhibiting two aspartate residues instead of these alanines (Fig. 5, *A* and *B*). This version of *Cc*Trx1 (*Cc*Trx1$_{DD}$) is no longer degraded in predivisional cells and accumulates in cells, confirming that the AA motif triggers protein degradation. Moreover, this accumulation masks the slight increase in *Cc*Trx1 expression observed in a WT strain in early S phase. Next, we tested the implication of the essential ClpXP machinery in this degradation using depletion strains. Depletion of ClpX or ClpP clearly showed an accumulation of *Cc*Trx1 compared with the WT strain (Fig. 5, *C* and *D*). Furthermore, a recent study showed that deleting a toxin–antitoxin system (the SocAB system) that requires ClpXP for toxin degradation alleviates the essentiality of the protease (27). Therefore, to corroborate our previous observations, we compared the levels of *Cc*Trx1 in Δ*socAB*, Δ*socAB*Δ*clpX*, and Δ*socAB*Δ*clpP* mutants. Once again, the clear increase in *Cc*Trx1 level in the *clpX* or *clpP* deletion strain confirmed that the ClpXP machinery is responsible for the degradation of *Cc*Trx1 in predivisional cells (Fig. 5*E*). Altogether, our results reveal that a complex regulatory mechanism, involving transcriptional control and protein degradation, confines high *Cc*Trx1 levels to the early S phase of the cell cycle.

Accumulation of CcTrx1 is toxic in C. crescentus

Trx proteins play beneficial roles for cells, and deleterious effects due to their presence have never been reported. However, the active degradation of *Cc*Trx1 by ClpXP suggests that accumulation of this protein could be toxic in *C. crescentus.* Therefore, we constructed an overexpressing strain (Δ*cctrx1*, pBX-cctrx1) to test the hypothesis that accumulating *Cc*Trx1 is damaging to cells. Accordingly, cells overexpressing *Cc*Trx1 (Fig. 6*A*) do not grow under normal conditions (Fig. 6*B*). Using 4-acetamido-4′-maleimidylstilbene-2,2′-disulfonic acid (AMS), an alkylating reagent that binds free thiols, thereby increasing the molecular weight of reduced proteins, we verified that overexpression of *Cc*Trx1 had no impact on the oxidation state of this protein *in vivo* (Fig. S2). Regardless of its expression level, *Cc*Trx1 was found to be mostly reduced.

Discussion

In this study, we report the characterization of *Cc*Trx1, a bacterial oxidoreductase that is essential for the growth and survival of *C. crescentus*. We show that the expression of *Cc*Trx1, a protein that exhibits all the characteristics of classical Trxs *in vitro*, is tightly regulated and that this regulation is important for cell growth.

The expression of *Cc*Trx1 is induced in early S phase concomitantly with the initiation of DNA replication and the expression of the two subunits of the ribonucleotide reductase (RNR) (6, 28). This essential enzyme is responsible for the reduction of ribonucleotides to their corresponding deoxyribonucleotides, the building blocks of DNA synthesis. To remain active, RNR needs to be recycled by a reducing protein (2, 3). In

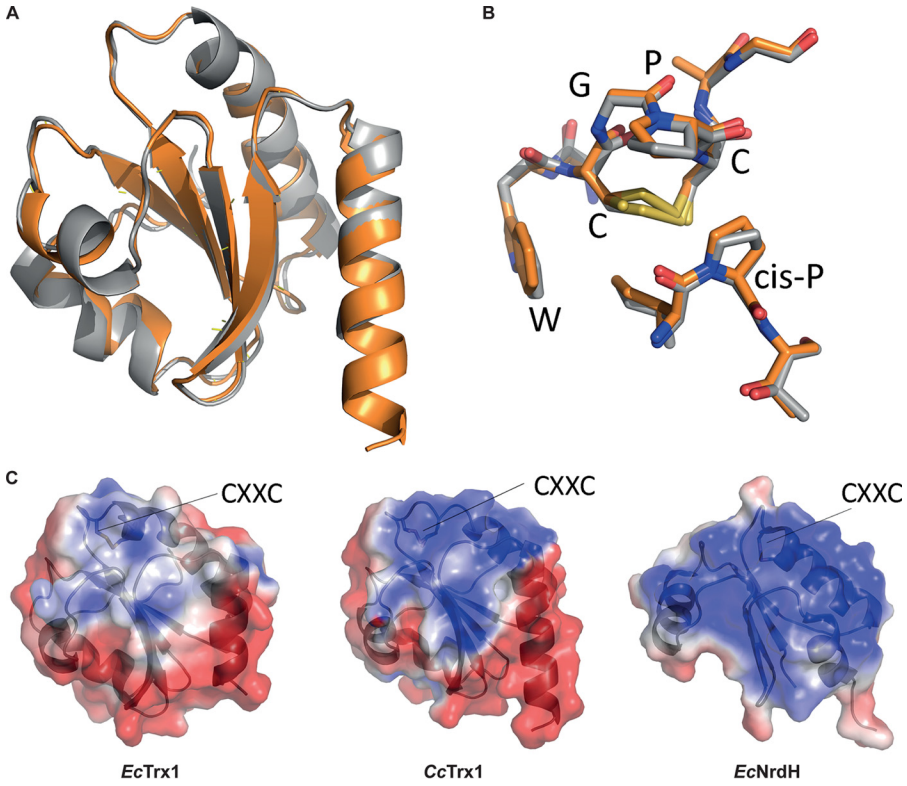

Figure 3. *Cc*Trx1 has a Trx fold with a positive surface potential in the substrate contact area. *A*, overlay of *Cc*Trx1 (Protein Data Bank code 6ESX; *orange*) with *Ec*Trx1 (Protein Data Bank code 2TRX; *gray*) shows a structurally conserved Trx fold. *B*, overlay of the active-site sequence motif of *Cc*Trx1 and *Ec*Trx1. *C*, electrostatic surface potentials (from −2 (*red*) to +2*kT*/*e* (*blue*)) mapped to the surface of *Ec*Trx1 (Protein Data Bank code 2TRX), *Cc*Trx1 (Protein Data Bank code 6ESX), and *Ec*NrdH (Protein Data Bank code 1H75). Figure panels were prepared with open-source PyMOL 1.8.x (*A* and *B*) and using Adaptive Poisson-Boltzmann Solver (APBS) tools after PDB2PQR file conversion (*C*).

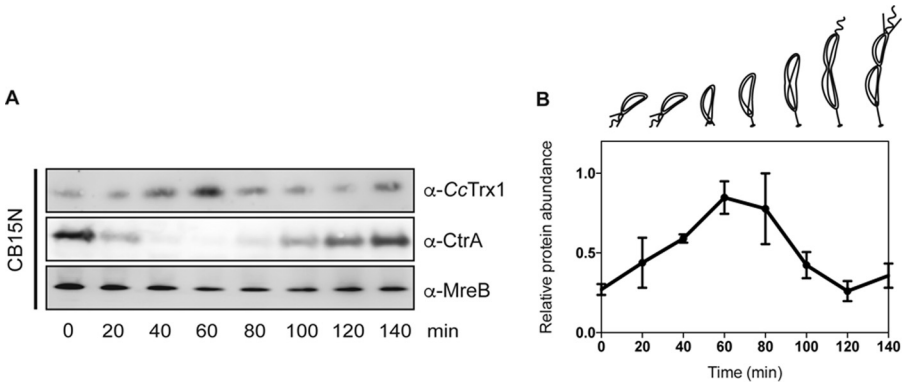

Figure 4. *Cc*Trx1 is cell cycle–regulated. *A*, a WT cell (CB15N) culture was synchronized, and samples were withdrawn every 20 min. Immunoblotting detection shows the levels of *Cc*Trx1 over the cell cycle. MreB is used as a loading control, and CtrA serves as a synchrony control. This experiment was performed in triplicate, and this panel shows representative results. The additional experiments are presented in Fig. S3. *B*, quantification of the levels of *Cc*Trx1. Bands were detected by immunoblotting and quantified using ImageJ. This graph shows the mean of three independent experiments. *Error bars* represent S.E.

E. coli, redundant proteins with Trx folds are capable of reducing RNR, thereby ensuring its constant activity (29). In contrast to fast-growing bacteria such as *E. coli*, *C. crescentus* constrains the energy-consuming process of DNA replication to occur only once per cell cycle during a well defined time window (Fig. 1). Previous large-scale studies showed that, in *C. crescentus*, RNR was expressed in early S phase (28) and degraded by the ClpXP protease (18). This expression pattern is similar to that of *Cc*Trx1, confining the expression of both proteins in early S phase and suggesting a functional connection. Furthermore, as the electrostatics of Trxs are determinant for substrate specificity (30), the more positive electrostatic surface of *Cc*Trx1 compared with *Ec*Trx1 might indicate that *Cc*Trx1 exhibits a function similar to *Ec*NrdH, another Trx-fold protein with a positive electrostatic surface (Fig. 3). This protein has a Grx-like structure but functions as a Trx and is the functional hydrogen donor of *Ec*NrdEF, an RNR present in the cytoplasm of *E. coli* (31, 32). Altogether, these observations strongly suggest that *Cc*Trx1 is the protein responsible for the reduction of RNR, which would explain its essentiality. Additionally, it is interesting to note that, in *C. crescentus*, the production of deoxyribonucleotides seems to be restricted to the early S phase of the cell cycle, uncovering another layer in the regulation of DNA replication initiation in this bacterium.

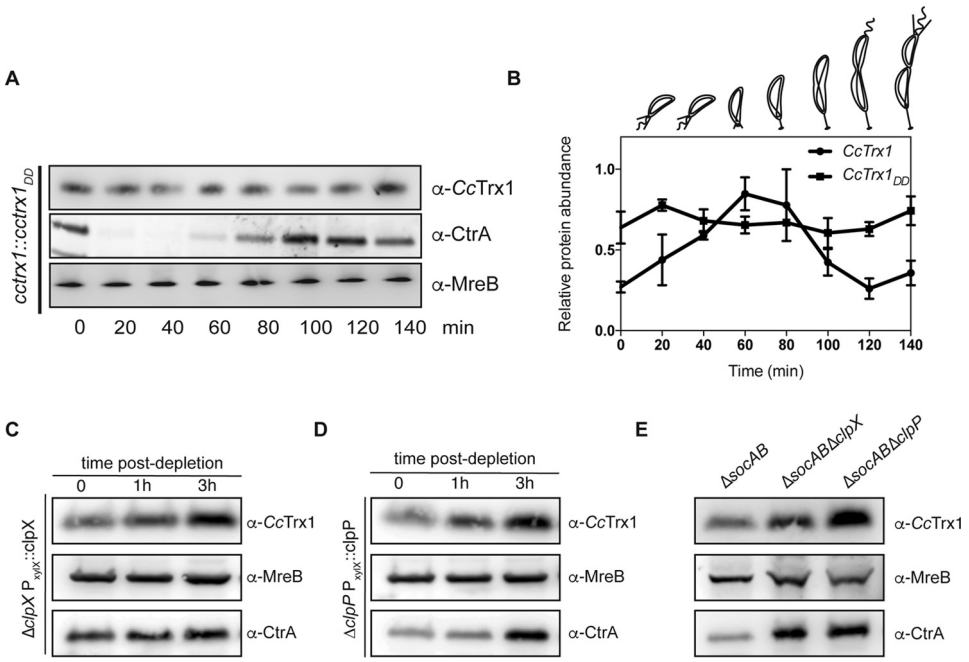

Figure 5. *Cc*Trx1 is degraded by the ClpXP machinery. *A*, in the *cctrx1*::*cctrx1*$_{DD}$ strain, the levels of *Cc*Trx1 do not fluctuate over the cell cycle. A culture was synchronized, and samples were withdrawn every 20 min. Immunoblotting detection shows the levels of *Cc*Trx1 over the cell cycle. MreB is used as a loading control, and CtrA serves as a synchrony control. This experiment was performed in triplicate, and this panel shows representative results. The additional experiments are present in Fig. S3. *B*, quantification of the levels of *Cc*Trx1. Bands were detected by immunoblotting and quantified using ImageJ. This graph shows the mean of three independent experiments. *Error bars* represent S.E. *C*, *Cc*Trx1 accumulates in a ClpX depletion strain. Δ*clpX xylX*::P$_{xyl}$-clpX cells were grown under permissive conditions before xylose was washed out to start the ClpX depletion. Samples were withdrawn after 1, 2, and 3 h. *Cc*Trx1 was detected by immunoblotting. MreB serves as a loading control, and CtrA is a known substrate of ClpXP. This experiment was performed in triplicate, and this panel shows representative results. *D*, *Cc*Trx1 accumulates in a ClpP depletion strain. Δ*clpP xylX*::P$_{xyl}$-clpP cells were grown under permissive conditions before xylose was washed out to start the ClpP depletion. Samples were withdrawn after 1, 2, and 3 h. *Cc*Trx1 was detected by immunoblotting. MreB serves as a loading control, and CtrA is a known substrate of ClpXP. This experiment was performed in triplicate, and this panel shows representative results. *E*, *Cc*Trx1 accumulates in the absence of ClpX or ClpP. The CB15N Δ*socAB*, CB15N Δ*socAB* Δ*clpX*, and CB15N Δ*socAB* Δ*clpP* mutants were grown until $A_{660\ nm}$ reached 0.3. *Cc*Trx1 levels were assessed by immunoblotting. MreB serves as a loading control, and CtrA is a known substrate of ClpXP. This experiment was performed in triplicate, and this panel shows representative results.

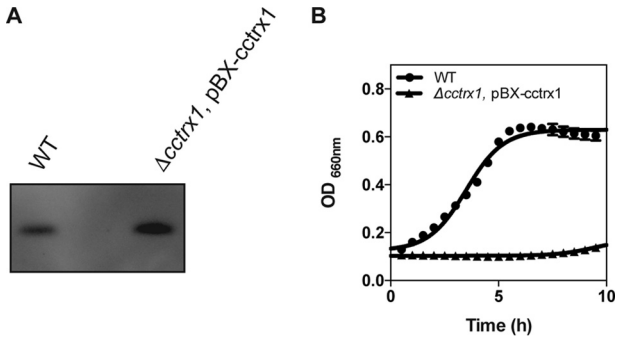

Figure 6. Overexpression of *Cc*Trx1. *A*, expression levels of *Cc*Trx1 in a WT and an overexpression strain (Δ*cctrx1* pBX-cctrx1). This experiment was performed in triplicate, and this panel shows representative results. *B*, the growth curves of a WT and an overexpression strain (Δ*cctrx1* pBX-cctrx1) show that accumulation of *Cc*Trx1 prevents cell growth. Cells were grown in M2G at 30 °C in a 96-well plate, and growth curves were monitored using a Biotek Synergy H1 Hybrid microplate reader. This graph shows the mean of three independent experiments. *Error bars* represent S.E.

Over the years, the ClpXP machinery has become a central player in the cell cycle progression of *C. crescentus*, which depends on spatially and temporally regulated proteolysis (17, 18). However, as ClpXP is constitutively expressed during the cell cycle, the mechanisms that govern its differential substrate recognition remain elusive. These are based, on the one hand, on the presence of specific adaptors that are only present for a precise moment of the cell cycle (26) and, on the other hand, on the subcellular localization of the ClpXP machinery itself. For example, during the G_1 to S transition, ClpXP localizes at the cell pole where it is responsible for the proteolysis of several polarly localized proteins, including flagellar components and CtrA, a master regulator in *C. crescentus* that prevents DNA replication (22–24). After DNA replication, ClpXP reaches the cell division ring to clear divisome components from the daughter swarmer cell (33, 34). How ClpXP recognizes *Cc*Trx1 as a substrate in predivisional cells is unclear. Our hypothesis is that, as *Cc*Trx1 is diffused in the cytoplasm (data not shown), it only encounters high concentrations of ClpXP in predivisional cells when the protease transits from the cell pole (G_1 to S transition) to the cell division ring (G_2).

Interestingly, the cell cycle of *C. crescentus* has recently been shown to be redox-regulated (8). Indeed, the redox state of the cytoplasm varies during the cell cycle: although this compartment is more reducing in G phase, it becomes more oxidizing in S phase before returning to more reducing conditions in G_2/M phase (8). Although oxidation is usually considered to be deleterious and leads to inactivation of numerous proteins, several regulatory proteins are directly or indirectly activated during this "oxidizing" phase (8, 19, 20). One example is NstA, a negative regulator of topoisomerase IV, which is activated by the formation of a disulfide bond during the "oxidative phase" of the cycle (8). In addition to its function in RNR recycling, *Cc*Trx1 might be required during this oxidative phase to pro-

tect sensitive cysteines in its substrates from this general oxidative state. After DNA replication, the cytoplasm becomes reducing again, and *Cc*Trx1 is no longer needed.

An intriguing result of our study is that constitutively overexpressing *Cc*Trx1 completely prevents cell growth. This is puzzling as Trxs are known to play beneficial roles in cells. One hypothesis to explain this perturbation is that in swarmer cells, which are normally devoid of *Cc*Trx1, the presence of this protein is deleterious. To us, this hypothesis seems unlikely because expressing a reducing protein in an already reducing environment (the cytoplasm of swarmer cells is reducing) should not be toxic. A second, more likely hypothesis is that accumulation of reduced *Cc*Trx1 in stalked cells, where it is normally present, could interfere with the oxidative activation of regulatory proteins (discussed above) and prevent the progression of the cell cycle. Interestingly, we note that the strain expressing $Cc\text{Trx1}_{DD}$, the non-degradable variant of *Cc*Trx1 that is expressed at physiological levels, did not display any growth defects under normal laboratory conditions (data not shown), thus suggesting that only a large accumulation of *Cc*Trx1 substantially perturbs cell cycle progression.

Here, we postulate that the tight regulation of *Cc*Trx1 allows *C. crescentus* to cope with changes in the intracellular redox environment during progression of the cell cycle. However, because *C. crescentus* does not encode a second Trx, this implies that the only Trx expressed by this organism is only present during a short window of time during the cell cycle. This is expected to make *C. crescentus* extremely sensitive to external oxidative stress compared with *E. coli*. However, the physiological relevance of this hypothesis, if correct, is unclear as *C. crescentus* and *E. coli* exhibit very different lifestyles and colonize very different habitats.

The asymmetry in the cell cycle of *C. crescentus* is thought to be an evolutionary advantage that ensures the persistence of two cell types, the swarmer and the stalked cells in the population. Stalked cells are non-motile and can form communities. If needed, they are able to defend themselves against a variety of stresses. Swarmer cells, in contrast, are motile and can afford to colonize new places. In case of stress, these cells are more sensitive but can flee from the source of stress. A recent study highlighted this bet-hedging strategy during copper stress (35). This bimodal response probably also applies to oxidative stress: the swarmer cells could easily escape from an oxidative environment, whereas the stalked cells would be able to defend themselves due to the presence of *Cc*Trx1.

Experimental procedures

Bacterial strains, media, and plasmids

All strains and plasmids used in this study are listed in Table S1. Growth conditions are specified below for each experiment. Cells were usually grown in M2G minimal medium (6.1 mM Na_2HPO_4, 3.9 mM KH_2PO_4, 9.3 mM NH_4Cl, 0.5 mM $MgSO_4$, 10 μM $FeSO_4$, 0.5 mM $CaCl_2$, 0.2% glucose). The CB15N WT *C. crescentus* strain, used in this study, is a strain that adapted to laboratory growth conditions and lost its ability to attach to surfaces. For more information on this strain, see Marks *et al.* (36).

Protein purification and antibody production

All purifications were performed using the ÄKTA Pure chromatography system. Both *Cc*Trx1 and *Cc*TrxR were expressed in *E. coli* BL21(DE3) from a pET23a plasmid, adding a His tag at their C termini. *Cc*Trx1 was amplified from CB15N chromosomal DNA using primers GAGCATATGATGAGCACCGTTGCG and CTCCTCGAGGGCGGCCTGGACGCC, and *Cc*TrxR was amplified from CB15N chromosomal DNA using primers GAGCATATGATGTCGCCACTGCGG and CTCCTCGAGCCAAACCCCGATCTTGTTGGCC. Both were inserted in the pET23a vector between the NdeI and XhoI restriction sites. After an overnight preculture, cells were diluted in 3 liters of LB containing 100 μg/ml ampicillin and grown at 37 °C in a shaking incubator. At midlog phase, expression was induced by addition of 1 mM isopropyl 1-thio-β-D-galactopyranoside for 3 h. Cells were then harvested; resuspended in 50 mM NaP_i, pH 8.0, 300 mM NaCl; and lysed using a French press. After centrifugation for 40 min at 23,000 × *g* at 4 °C, the supernatant was loaded onto a 5-ml HisTrap HP (GE Healthcare). Both proteins were eluted by a gradient containing 0–40% buffer B (50 mM NaP_i, pH 8.0, 300 mM NaCl, 300 mM imidazole). *Cc*Trx1 and *Cc*TrxR were then subjected to a second step of purification using a HiLoad S75 16/60 gel filtration column (GE Healthcare) and eluted in 10 mM HEPES-KOH, pH 8.0, 100 mM NaCl. After these two steps, both *Cc*Trx1 and *Cc*TrxR were pure and could be used to perform biochemical tests. *Cc*Trx1 was also used to produce antibodies (rabbit serum; CER Groupe, Belgium) and for crystallization experiments (see below).

CcTrx1 alignment

*Cc*Trx1 (accession number YP_002519026.1) was aligned with Trx1 from *E. coli* (accession number NP_418228.2), *Saccharomyces cerevisiae* (accession number P22217), and *Homo sapiens* (accession number P10599.3) using MacVector 12.0.1.

Insulin reduction assay

The insulin reduction assay was performed as published previously (9). Briefly, 150 μM insulin and 10 μM tested protein (either *Cc*Trx1 or *Ec*Trx1) were mixed in 100 mM potassium phosphate, pH 7.0, 1 mM EDTA. The reaction was initiated by addition of a final concentration of 0.8 mM DTT, and the reduction of insulin was monitored at 650 nm using a spectrophotometer (Varian Cary 50 UV-visible).

Redox potential

*Cc*Trx1 (1 μM) was incubated overnight at room temperature in 50 mM potassium buffer, pH 7.0, 0.1 mM EDTA and various ratios of DTT_{ox}/DTT_{red}. The protein was then precipitated with 10% trichloroacetic acid. After 20 min of incubation on ice, the samples were centrifuged (16,100 × *g*, 5 min, 4 °C), and the pellets were washed with cold acetone. After a second centrifugation step, pellets were dried and resuspended in non-reducing SDS sample buffer (2% SDS, 10% glycerol, 0.002% bromphenol blue, 0.062 M Tris-HCl, pH 6.8) containing 20 mM AMS. After 45 min at 37 °C, samples were loaded for SDS-PAGE (NuPAGE Bis-Tris 12%, Thermo Fisher Scientific) and colored

by PageBlue protein staining solution (Thermo Scientific). Ratios of oxidized and reduced proteins were determined by ImageJ, and the redox potential was calculated as described previously (37).

K_m determination

*Cc*Trx1 was first oxidized with 40 mM diamide (Sigma-Aldrich) for 30 min at 37 °C. The diamide was then removed using a desalting column (Nap-5, GE Healthcare). 200 μM NADPH, 1.25 μM *Cc*TrxR, and various concentrations of oxidized *Cc*Trx1 (0, 0.1, 0.5, 1, 2, and 5 μM) were mixed, and the absorbance of this mixture was followed at 340 nm for 3 min using a spectrophotometer. Then the rate of substrate reduction was calculated (μmol/(min $\times$ μg of protein)) knowing the extinction coefficient of NADPH ($\epsilon = 6220\ M^{-1}\ cm^{-1}$) and that for 1 eq of NADPH oxidized 1 eq of substrate is reduced.

Crystallization, X-ray diffraction, and structure determination of CcTrx1

*Cc*Trx1 was purified as explained above. An additional purification step was needed to obtain a homogeneous sample. *Cc*Trx1 was injected on a preparative Jupiter C_4 reverse-phase column (10 μm, 300 Å, 10 $\times$ 250 mm; Phenomenex, CA) equilibrated in 20 mM Tris-HCl, pH 8, 0.1 M KCl, 1 mM DTT and eluted with a linear gradient of acetonitrile in the same buffer. The sample was then dialyzed against 20 mM HEPES-NaOH, pH 7.5, 150 mM NaCl. *Cc*Trx1 was concentrated to 18.6 mg/ml, and initial crystallization conditions were screened using the Molecular Dimensions structure screen using the hanging-drop vapor-diffusion technique at 20 °C. After 1 day, small crystals were obtained in 0.1 M sodium citrate, pH 5.6, 20% 2-propanol, 20% PEG 4000. By decreasing the protein concentration to 7 mg/ml, we obtained nice, needle shaped crystals. The crystals were frozen in 20% glycerol, 0.1 M sodium citrate, pH 5.6, 20% 2-propanol, 20% PEG 4000 as cryoprotectant.

X-ray diffraction data were collected at the Proxima 2 beamline at the Soleil synchrotron facility. The data were processed using the XDS package (38). The structure of *Cc*Trx1 was solved using molecular replacement using the *Acetobacter aceti* Trx (Protein Data Bank code 2I4A; 58% sequence identity) as a search model using the Phaser program (39) from the PHENIX suite (40). The sequence of *Cc*Trx1 was built in the initial electron density using AutoBuild (41) from the same suite. The structure was inspected and further built manually using Coot (42) and refined using phenix.refine (43). The structures were deposited to the Protein Data Bank under accession code 6ESX. X-ray data collection parameters, processing, and refinement statistics are summarized in Table 1.

Knockout

The knockout was built using a two-step recombination method. The upstream and downstream regions of *cctrx1* were amplified (upstream, gaggatatctggccatggccagcgcggcgtttg and ctcgctagccgcaacggtgctcatggtctgctc; downstream, gaggctagcggcgtccaggccgcctaagcggc and ctctccggatccagctggagccggcccc) from CB15N chromosomal DNA and cloned together into pNPTS138 vector to create an in-frame deletion. This plasmid was transformed in *C. crescentus* by electroporation, plated on PYE (0.2% w/v Bacto peptone, 0.1% (w/v) yeast extract, 1 mM $MgSO_4$, 0.5 mM $CaCl_2$)-kanamycin (final concentration, 20 μg/ml) to select for plasmid integration, and incubated at 30 °C for 2 days. A few integrants were inoculated in PYE without selection and grown at 30 °C to allow the second recombination to occur before plating on PYE plates containing 3% sucrose to select for cells that lost the plasmid (*sacB* counterselection). Plates were incubated at 30 °C for 2 days. The clones obtained were patched onto a PYE plate and PYE-kanamycin plate to select for clones that effectively lost the plasmid and not those with an inactivated copy of *sacB.* The knockout construct was then verified by PCR using primers (gaggatatctggccatggccagcgcggcgtttg and ctctccggatccagctggagccggcccc) upstream and downstream of *cctrx1.*

Synchrony

This protocol was adapted from Ely (14). Briefly, a preculture was grown overnight in M2G at 30 °C and diluted in 400 ml of M2G. When the $A_{660\ nm}$ reached 0.3, cells were harvested by centrifugation (8,000 $\times$ *g*, 15 min, 4 °C) and resuspended in 45 ml of M2 salts (6.1 mM Na_2HPO_4, 3.9 mM KH_2PO_4, 9.3 mM NH_4Cl, 0.5 mM $MgSO_4$, 10 μM $FeSO_4$, 0.5 mM $CaCl_2$) (14) and 15 ml of Ludox (Sigma-Aldrich). Samples were transferred to Corex tubes and centrifuged at 24,300 $\times$ *g* for 30 min at 4 °C. After this centrifugation, two distinct bands appeared in the Ludox gradient, the lower band corresponding to the swarmer cells. This band was collected and washed in 30 ml of M2 salts (centrifugation, 15 min, 21,600 $\times$ *g*, 4 °C). The pellet was collected and transferred to an Eppendorf tube before being washed two times in M2 salts (centrifugation, 1 min, 4 °C, 10,000 $\times$ *g*). The pellet was diluted in prewarmed (30 °C) M2G to reach an $A_{660\ nm}$ of 0.2–0.3. Every 20 min, 1 ml of sample was withdrawn, centrifuged, and resuspended in SDS sample buffer (volume normalized by OD). Samples were then heated at 95 °C for 10 min and loaded for SDS-PAGE (NuPAGE Bis-Tris 12%). Proteins were detected by Western blotting using α-*Cc*Trx1 (CER Groupe; dilution, 1:500), α-MreB, or α-CtrA (both received from R. Hallez, Université de Namur; dilution, 1:2000) antibody.

Depletion of ClpX and ClpP

The depletion strains harboring a xylose-inducible promoter upstream of either *clpX* or *clpP* were grown at 30 °C in M2G until reaching an $A_{660\ nm}$ of 0.3 in the presence of 0.3% xylose. Then cells were washed to remove the xylose and grown at 30 °C in M2G for 3 h. 1 ml of sample was withdrawn, centrifuged, and resuspended in SDS sample buffer (volume normalized by OD) every hour. Samples were then heated at 95 °C for 10 min and loaded for SDS-PAGE (NuPAGE Bis-Tris 12%). Proteins were detected by Western blotting using α-*Cc*Trx1 (dilution, 1:500), α-MreB, or α-CtrA (dilution, 1:2000) antibody.

Growth curves

Cells (WT, FB17) were grown overnight in 5 ml of M2G under permissive conditions: no xylose and 2 μg/ml gentamycin for the overexpression strain. Cells were then diluted (1:50) in M2G (with 0.3% xylose and 2 μg/ml gentamycin for the over-

expression strain). 200 μl of culture were transferred to a 96-well plate. The growth ($A_{660\ nm}$) was then followed for 10 h at 30 °C using a Biotek Synergy H1 Hybrid microplate reader.

Thiol-trapping experiment

The *in vivo* redox state of *Cc*Trx1 was assessed using AMS trapping experiments as described by Denoncin *et al.* (44). Briefly, bacteria were cultured at 30 °C until an $A_{660\ nm}$ of 0.3 was reached. If needed, *Cc*Trx1 was induced with 0.3% xylose for 2 h. The proteins were then TCA-precipitated (10% cold TCA) and resuspended in 30 μl of 20 mM AMS, 0.1% SDS, 10 mM EDTA, 50 mM Tris-HCl, pH 7.5. Samples were incubated for 45 min at 37 °C protected from light. As a positive control, protein pellets were treated with 50 mM DTT in the presence of 200 mM Tris, pH 8, 1% SDS. Samples were separated by 12% SDS-PAGE and detected by Western blotting (anti-*Cc*Trx1 antibody).

Author contributions—C. V. G. and J.-F. C. conceptualization; C. V. G. formal analysis; C. V. G. validation; C. V. G., F. B., K. W., and I. V. M. investigation; C. V. G., F. B., and J. M. methodology; C. V. G. and J.-F. C. writing-original draft; C. V. G., F. B., I. V. M., J. M., and J.-F. C. writing-review and editing; J. M. and J.-F. C. supervision; J. M. and J.-F. C. funding acquisition; J.-F. C. project administration.

Acknowledgments—We thank Pauline Leverrier for critically reading our manuscript. We thank the members of the laboratory for helpful discussions. We thank the staff of the Proxima 2 beamline at the Soleil synchrotron facility.

References

1. Collet, J. F., and Messens, J. (2010) Structure, function, and mechanism of thioredoxin proteins. *Antioxid. Redox Signal.* **13,** 1205–1216 CrossRef Medline
2. Laurent, T. C., Moore, E. C., and Reichard, P. (1964) Enzymatic synthesis of deoxyribonucleotides. IV. Isolation and characterization of thioredoxin, the hydrogen donor from *Escherichia coli* B. *J. Biol. Chem.* **239,** 3436–3444 Medline
3. Moore, E. C., Reichard, P., and Thelander, L. (1964) Enzymatic synthesis of deoxyribonucleotides. V. Purification and properties of thioredoxin reductase from *Escherichia coli* B. *J. Biol. Chem.* **239,** 3445–3452 Medline
4. Arts, I. S., Vertommen, D., Baldin, F., Laloux, G., and Collet, J. F. (2016) Comprehensively characterizing the thioredoxin interactome *in vivo* highlights the central role played by this ubiquitous oxidoreductase in redox control. *Mol. Cell. Proteomics* **15,** 2125–2140 CrossRef Medline
5. Christen, B., Abeliuk, E., Collier, J. M., Kalogeraki, V. S., Passarelli, B., Coller, J. A., Fero, M. J., McAdams, H. H., and Shapiro, L. (2011) The essential genome of a bacterium. *Mol. Syst. Biol.* **7,** 528CrossRef Medline
6. Hottes, A. K., Shapiro, L., and McAdams, H. H. (2005) DnaA coordinates replication initiation and cell cycle transcription in *Caulobacter crescentus*. *Mol. Microbiol.* **58,** 1340–1353 CrossRef Medline
7. Curtis, P. D., and Brun, Y. V. (2010) Getting in the loop: regulation of development in *Caulobacter crescentus*. *Microbio.l Mol. Biol. Rev.* **74,** 13–41 CrossRef Medline
8. Narayanan, S., Janakiraman, B., Kumar, L., and Radhakrishnan, S. K. (2015) A cell cycle-controlled redox switch regulates the topoisomerase IV activity. *Genes Dev.* **29,** 1175–1187 CrossRef Medline
9. Holmgren, A. (1979) Thioredoxin catalyzes the reduction of insulin disulfides by dithiothreitol and dihydrolipoamide. *J. Biol. Chem.* **254,** 9627–9632 Medline
10. Krause, G., and Holmgren, A. (1991) Substitution of the conserved tryptophan 31 in *Escherichia coli* thioredoxin by site-directed mutagenesis and structure-function analysis. *J. Biol. Chem.* **266,** 4056–4066 Medline
11. Chivers, P. T., Prehoda, K. E., and Raines, R. T. (1997) The CXXC motif: a rheostat in the active site. *Biochemistry* **36,** 4061–4066 CrossRef Medline
12. Jordan, A., Aslund, F., Pontis, E., Reichard, P., and Holmgren, A. (1997) Characterization of *Escherichia coli* NrdH. A glutaredoxin-like protein with a thioredoxin-like activity profile. *J. Biol. Chem.* **272,** 18044–18050 CrossRef Medline
13. Lu, J., and Holmgren, A. (2014) The thioredoxin antioxidant system. *Free Radic. Biol. Med.* **66,** 75–87 CrossRef Medline
14. Ely, B. (1991) Genetics of *Caulobacter crescentus*. *Methods Enzymol.* **204,** 372–384 CrossRef Medline
15. Flynn, J. M., Neher, S. B., Kim, Y. I., Sauer, R. T., and Baker, T. A. (2003) Proteomic discovery of cellular substrates of the ClpXP protease reveals five classes of ClpX-recognition signals. *Mol. Cell* **11,** 671–683 CrossRef Medline
16. Alexopoulos, J. A., Guarné, A., and Ortega, J. (2012) ClpP: a structurally dynamic protease regulated by AAA+ proteins. *J. Struct. Biol.* **179,** 202–210 CrossRef Medline
17. Jenal, U. (2009) The role of proteolysis in the *Caulobacter crescentus* cell cycle and development. *Res. Microbiol.* **160,** 687–695 CrossRef Medline
18. Bhat, N. H., Vass, R. H., Stoddard, P. R., Shin, D. K., and Chien, P. (2013) Identification of ClpP substrates in *Caulobacter crescentus* reveals a role for regulated proteolysis in bacterial development. *Mol. Microbiol.* **88,** 1083–1092 CrossRef Medline
19. Radhakrishnan, S. K., Pritchard, S., and Viollier, P. H. (2010) Coupling prokaryotic cell fate and division control with a bifunctional and oscillating oxidoreductase homolog. *Dev. Cell* **18,** 90–101 CrossRef Medline
20. Beaufay, F., Coppine, J., Mayard, A., Laloux, G., De Bolle, X., and Hallez, R. (2015) A NAD-dependent glutamate dehydrogenase coordinates metabolism with cell division in *Caulobacter crescentus*. *EMBO J.* **34,** 1786–1800 CrossRef Medline
21. Tsai, J. W., and Alley, M. R. (2001) Proteolysis of the *Caulobacter* McpA chemoreceptor is cell cycle regulated by a ClpX-dependent pathway. *J. Bacteriol.* **183,** 5001–5007 CrossRef Medline
22. Domian, I. J., Quon, K. C., and Shapiro, L. (1997) Cell type-specific phosphorylation and proteolysis of a transcriptional regulator controls the G1-to-S transition in a bacterial cell cycle. *Cell* **90,** 415–424 CrossRef Medline
23. Jenal, U., and Fuchs, T. (1998) An essential protease involved in bacterial cell-cycle control. *EMBO J.* **17,** 5658–5669 CrossRef Medline
24. McGrath, P. T., Iniesta, A. A., Ryan, K. R., Shapiro, L., and McAdams, H. H. (2006) A dynamically localized protease complex and a polar specificity factor control a cell cycle master regulator. *Cell* **124,** 535–547 CrossRef Medline
25. Iniesta, A. A., McGrath, P. T., Reisenauer, A., McAdams, H. H., and Shapiro, L. (2006) A phospho-signaling pathway controls the localization and activity of a protease complex critical for bacterial cell cycle progression. *Proc. Natl. Acad. Sci. U.S.A.* **103,** 10935–10940 CrossRef Medline
26. Joshi, K. K., and Chien, P. (2016) Regulated proteolysis in bacteria: *Caulobacter*. *Annu. Rev. Genet.* **50,** 423–445 CrossRef Medline
27. Markovski, M., and Wickner, S. (2013) Preventing bacterial suicide: a novel toxin-antitoxin strategy. *Mol. Cell* **52,** 611–612 CrossRef Medline
28. Hottes, A. K., Meewan, M., Yang, D., Arana, N., Romero, P., McAdams, H. H., and Stephens, C. (2004) Transcriptional profiling of *Caulobacter crescentus* during growth on complex and minimal media. *J. Bacteriol.* **186,** 1448–1461 CrossRef Medline
29. Sengupta, R., and Holmgren, A. (2014) Thioredoxin and glutaredoxin-mediated redox regulation of ribonucleotide reductase. *World J. Biol. Chem.* **5,** 68–74 CrossRef Medline
30. Berndt, C., Schwenn, J.-D., and Lillig, C. H. (2015) The specificity of thioredoxins and glutaredoxins is determined by electrostatic and geometric complementarity. *Chem. Sci.***6,** 7049–7058 CrossRef
31. Stehr, M., Schneider, G., Aslund, F., Holmgren, A., and Lindqvist, Y. (2001) Structural basis for the thioredoxin-like activity profile of the glutaredoxin-like NrdH-redoxin from *Escherichia coli*. *J. Biol. Chem.* **276,** 35836–35841 CrossRef Medline

32. Gon, S., Faulkner, M. J., and Beckwith, J. (2006) *In vivo* requirement for glutaredoxins and thioredoxins in the reduction of the ribonucleotide reductases of *Escherichia coli*. *Antioxid. Redox Signal.* **8,** 735–742 CrossRef Medline
33. Kelly, A. J., Sackett, M. J., Din, N., Quardokus, E., and Brun, Y. V. (1998) Cell cycle-dependent transcriptional and proteolytic regulation of FtsZ in *Caulobacter*. *Genes Dev.* **12,** 880–893 CrossRef Medline
34. Martin, M. E., Trimble, M. J., and Brun, Y. V. (2004) Cell cycle-dependent abundance, stability and localization of FtsA and FtsQ in *Caulobacter crescentus*. *Mol. Microbiol.* **54,** 60–74 CrossRef Medline
35. Lawarée, E., Gillet, S., Louis, G., Tilquin, F., Le Blastier, S., Cambier, P., and Matroule, J. Y. (2016) *Caulobacter crescentus* intrinsic dimorphism provides a prompt bimodal response to copper stress. *Nat. Microbiol.* **1,** 16098 CrossRef Medline
36. Marks, M. E., Castro-Rojas, C. M., Teiling, C., Du, L., Kapatral, V., Walunas, T. L., and Crosson, S. (2010) The genetic basis of laboratory adaptation in *Caulobacter crescentus*. *J Bacteriol* **192,** 3678–3688 CrossRef Medline
37. Wunderlich, M., and Glockshuber, R. (1993) Redox properties of protein disulfide isomerase (DsbA) from *Escherichia coli*. *Protein Sci* **2,** 717–726 CrossRef Medline
38. Kabsch, W. (2010) XDS. *Acta Crystallogr. D Biol. Crystallogr.* **66,** 12 CrossRef5–132 Medline
39. McCoy, A. J., Grosse-Kunstleve, R. W., Adams, P. D., Winn, M. D., Storoni, L. C., and Read, R. J. (2007) Phaser crystallographic software. *J. Appl. Crystallogr.* **40,** 658–674 CrossRef
40. Adams, P. D., Afonine, P. V., Bunkóczi, G., Chen, V. B., Davis, I. W., Echols, N., Headd, J. J., Hung, L.-W., Kapral, G. J., Grosse-Kunstleve, R. W., McCoy, A. J., Moriarty, N. W., Oeffner, R., Read, R. J., Richardson, D. C., *et al.* (2010) PHENIX: a comprehensive Python-based system for macromolecular structure solution. *Acta Crystallogr. D Biol. Crystallogr.* **66,** 213–221 CrossRef Medline
41. Terwilliger, T. C., Grosse-Kunstleve, R. W., Afonine, P. V., Moriarty, N. W., Zwart, P. H., Hung, L.-W., Read, R. J., and Adams, P. D. (2008) Iterative model building, structure refinement and density modification with the PHENIX AutoBuild wizard. *Acta Crystallogr. D Biol. Crystallogr.* **64,** 61–69 CrossRef Medline
42. Emsley, P., and Cowtan, K. (2004) Coot: model-building tools for molecular graphics. *Acta Crystallogr. D Biol. Crystallogr.* **60,** 2126–2132 CrossRef Medline
43. Afonine, P. V., Grosse-Kunstleve, R. W., Echols, N., Headd, J. J., Moriarty, N. W., Mustyakimov, M., Terwilliger, T. C., Urzhumtsev, A., Zwart, P. H., and Adams, P. D. (2012) Towards automated crystallographic structure refinement with phenix.refine. *Acta Crystallogr. D Biol. Crystallogr.* **68,** 352–367 CrossRef Medline
44. Denoncin, K., Nicolaes, V., Cho, S. H., Leverrier, P., and Collet, J. F. (2013) Protein disulfide bond formation in the periplasm: determination of the *in vivo* redox state of cysteine residues. *Methods Mol. Biol.* **966,** 325–336 CrossRef Medline